RADIO MEASUREMENTS OF CORONAL MAGNETIC FIELDS

Stephen M. White

Dept. of Astronomy, Univ. of Maryland, College Park, MD 20742 USA

ABSTRACT

The measurement of magnetic field strengths in the solar corona using radio observations is reviewed. This is a well established technique that exploits the fact that the electron gyrofrequency for typical coronal magnetic field strengths (100–2000 Gauss) lies in the radio frequency range. Opacity from the resulting gyroresonance emission from hot plasma above active regions allows the direct measurement of the field strength, while some information on the direction of the magnetic field can be obtained from polarization measurements. In addition to the gyroresonance technique which works for strong fields above active regions, other measurements, such as the polarization of bremsstrahlung, also can provide information on weaker quiet–Sun fields. This paper is intended as a text version of the presentation, and in particular citations are not intended to be complete.

Key words: Coronal magnetic fields; Solar radio emission.

1. INTRODUCTION

When it comes to measuring coronal magnetic fields, radio astronomers benefit from what might be called the "anthroporadiomorphic" principle: *the range of magnetic field strengths in the corona is such that electrons gyrate under the Lorentz force about the magnetic field at frequencies exactly in the band easily accessible to radio astronomers from the ground*. This makes the radio regime the natural wavelength range to use to measure coronal magnetic field strengths, and nature provides us with a simple mechanism to take advantage of this fact: gyroresonance opacity, provided by the acceleration of thermal electrons in circular motion about the magnetic field, is sufficient to make the corona optically thick and such regions stand out in radio images by virtue of their million–degree brightness temperatures.

In addition to the direct effect of magnetic fields in producing opacity, they also affect radio emission through their influence on the response of the coronal plasma to electromagnetic fields, determining wave properties such as refractive index and polarization. As we will discuss, measuring the polarization of radio emission is one of the keys to unlocking the information it contains on coronal magnetic fields. One simplification is that we can generally ignore linear polarization of the radio emission, for two reasons: the natural electromagnetic modes in the coronal plasma are circularly–polarized, unless the radiation is propagating nearly orthogonal to the magnetic field; and Faraday rotation of the plane of linear polarization is so large and frequency–dependent that it is washed out when the radio emission is summed over any normal observing bandwidth.

Figure 1 demonstrates the appearance of the Sun at radio wavelengths. Virtually every feature of the solar corona is visible in radio images at some wavelength, thanks to the four well–understood emission mechanisms that dominate radio emission:

- *Bremsstrahlung* from thermal plasma, where the opacity is provided by collisions of electrons with ions, occurs throughout the solar atmosphere and is the dominant mechanism in most of the corona. It is optically thin above a few GHz and usually weakly polarized due to the response of the plasma. Since bremsstrahlung opacity depends on the plasma density as n_e^2, this mechanism is really a density diagnostic.
- *Gyroresonance emission* (emission from nonrelativistic thermal plasma at low harmonics of the electron gyrofrequency, $f_B = 2.8\,B$ MHz) is strong wherever $B > 300$ G in the corona and produces optically thick emission in active regions which may be highly polarized.
- *Gyrosynchrotron emission* (emission by mildly relativistic electrons at harmonics 10-100 of the gyrofrequency) is produced by nonthermal electrons in flares. Because the width of an individual resonance depends on $T_e/m_e c^2$, where T_e is the electron temperature, the resonances are very narrow for thermal emisison at coronal temperatures but broad for mildly relativistic electrons, so that in gyrosynchrotron emission resonances greatly overlap and

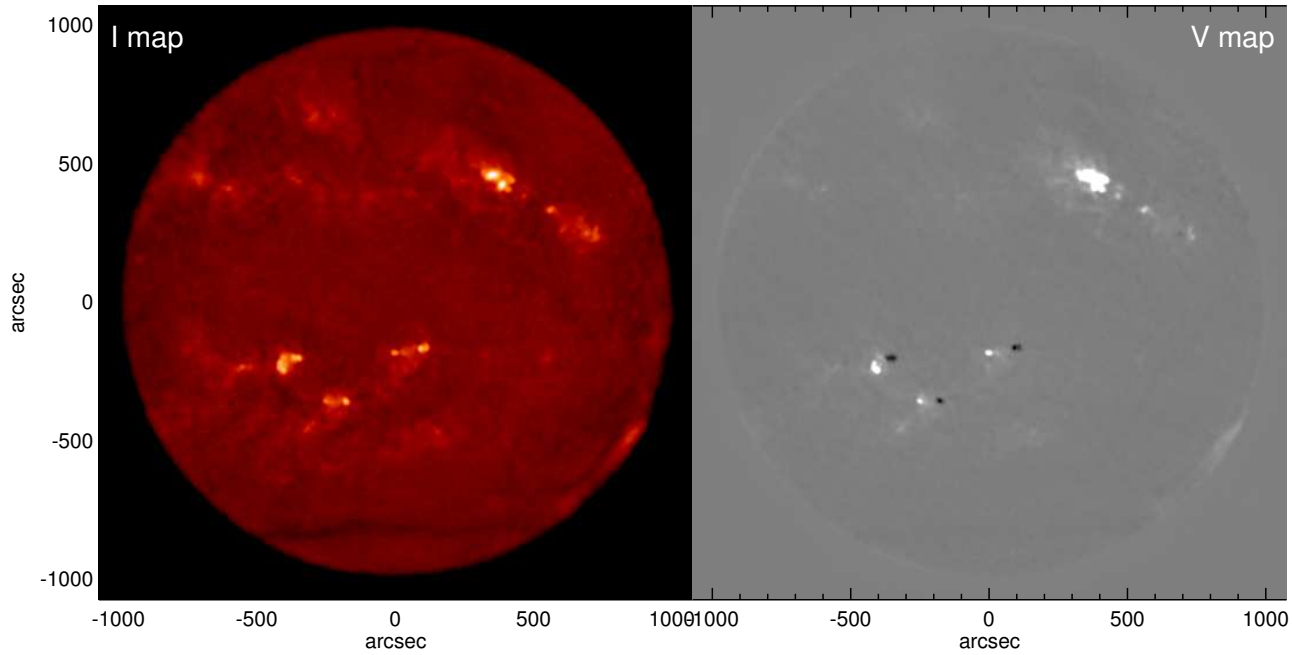

Figure 1. A radio image of the Sun at 4.6 GHz showing total intensity (Stokes I, left) and circular polarization (i.e., Stokes V, right). This image was made by pointing the Very Large Array at 23 different fields (each of 10′ diameter) and deconvolving the data jointly. The spatial resolution is 12″.

this is effectively a broadband mechanism. Circular polarization can be significant when the source is viewed along the magnetic field direction, while opacity is maximized when the source is viewed orthogonal to the magnetic field direction.

- *Plasma emission* when electrostatic Langmuir waves produced by energetic electrons with an unstable velocity distribution are converted to electromagnetic waves at the plasma frequency, f_p = 9000 $\sqrt{n_e}$, and its second harmonic. This mechanism is coherent and produces highly polarized bursts with very high brightness temperatures (in excess of the energies of the radiating elecrons). However, it is strongly suppressed by collisional absorption in the ambient plasma and thus is generally confined to low frequencies (1 GHz and below). In the presence of magnetic fields, fundamental plasma emission is highly polarized.

Because radio wavelengths are in the Rayleigh–Jeans limit (i.e., well to the long wavelength side of the thermal peak in the electromagnetic spectrum), the radio brightness temperature on the sky is proportional to the temperature of the source: $T_B = (1 - e^{-\tau})T_e$, where τ is the optical depth through the source. In particular, wherever the atmosphere is optically thick to radio emission, the observed radio brightness temperature is the actual temperature of the electrons which produce the emission. This fact provides a useful tool: any feature which is observed to have a coronal brightness temperature is therefore optically thick.

Most of the emission features visible in Fig. 1, where essentially all the visible structure is real, are due to bremsstrahlung from the densest plasma in the corona. The background disk is due to the fact that the observing frequency of 4.6 GHz, the solar atmosphere is optically thick in the upper chromosphere due to thermal bremsstrahlung at a layer where the temperature is about 20000 K. There is also a significant contribution to the disk from the optically thin quiet corona. This and the presence of spicules at the limb makes the radio disk significantly bigger than the photospheric disk (by about 30″ at this frequency). The corona is optically thin to bremsstrahlung everywhere at this frequency, so density contrast shows up very well in the total intensity map: low–density coronal features include the filament channel across the south polar region as well as elsewhere, where brightness temperatures are of order 7000 K below disk level, while brighter features are seen over plage near active regions (where the brightness temperature is typically 50000–100000 K). However, the brightest features are over sunspots in active regions where the brightness temperatures are in excess of 10^6 K: these are locations where the magnetic field in the corona is large enough to make the corona optically thick, requiring about 600 G at this frequency. The circular polarization image shows that these gyroresonance sources are highly polarized, and they reflect the orientation of the magnetic field in the corona: where the field in the source points towards us, the circular polarization is positive (right–circular–polarization dominates), and where the magnetic field points away from us the circular polarization is negative.

Figure 2 further illustrates the fact that radio emission from active regions is dominated by coronal mag-

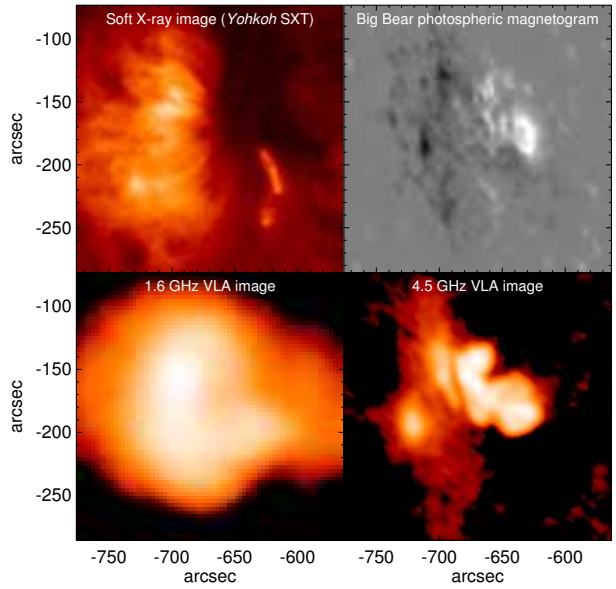

Figure 2. Portrait of a solar active region at four different wavelengths: soft X–rays (top left), photospheric magnetogram (top right, from Big Bear Solar Observatory), radio emission at 1.4 GHz (lower left) and at 4.6 GHz (lower right).

netic fields at frequencies above a few GHz. At lower frequencies, such as 1.4 GHz in the image shown, bremsstrahlung is generally optically thick over significant active regions because of the f^{-2} dependence of bremsstrahlung opacity, and the optically thick layer often lies above the corresponding optically thick level due to gyroresonance emission which is therefore not seen in the images. Thus the 1.4 GHz radio image closely resembles the soft X–ray image, which is also dominated by density contrast. However as frequency rises bremsstrahlung becomes optically thin and the radio image no longer looks like the soft X–ray image: rather, it more closely resembles a photospheric magnetogram (as in the 4.6 GHz image in Fig. 2) because the brightest features are now gyroresonance emission from regions where the magnetic field exceeds 600 G in the corona.

2. GYRORESONANCE EMISSION

A collisionless plasma such as the solar corona (where a typical collision frequency, e.g., for a density of n_e = 10^{10} cm^{-3} and temperature $T = 2 \times 10^6$ K, is 200 Hz) may be characterized by two frequencies corresponding to electron resonances: the frequency of oscillation of electrons in the electric field of the ions, known as the plasma frequency, $f_p = 8980\sqrt{n_e}$ Hz; and the gyro frequency, which is the frequency of rotation of an electron about the magnetic field due to the $\mathbf{v} \times \mathbf{B}$ Lorentz force, $f_B = 2.80 \times 10^6\, B$ Hz, where B is measured in G. For typical conditions in gyroresonant sources above active regions ($n_e = 10^{10}$ cm^{-3} and $B > 300$ G), $f_B > f_p$. In such a plasma the propagating electromagnetic modes corresponding to the free-space radiation modes are circularly polarized under most conditions. One of the modes, known as the *extraordinary* or x mode, gyrates about the magnetic field with the same sense of rotation as an electron, and therefore resonates strongly with the thermal electron population; the other mode, known as the *ordinary* or o mode, gyrates about the magnetic field direction with the sense opposite to that of the electron, and correspondingly interacts much less strongly. Since a radio telescope can generally detect both modes independently, as opposite circular polarizations, this difference in the strength of interaction of the two modes provides a powerful diagnostic.

The frequency width of a given cyclotron resonance $\propto \mu^{-1/2} s f_B$, where $\mu = m_e c^2/k_B T$. Since $\mu \approx 3000$ in the corona, the cyclotron resonances are very narrow and, for a given value of f_B, opacity is only significant at frequencies very close to discrete harmonics sf_B, s = 1,2,3,... (at much higher temperatures the individual resonances have significant width and may overlap). Equivalently, if we are observing an inhomogeneous corona at a frequency f, gyroresonance opacity is only significant at those discrete points along the line of sight at which $f_B = f/s$, s = 1,2,3,... The thermal width of the cyclotron resonance at coronal temperatures is such that B varies by less than 2% across a resonant layer, corresponding to a physical width of less than 200 km for typical coronal magnetic gradients (scale length $\sim 10^4$ km). The narrow physical thickness of the gyroresonant layers is an important feature of this mechanism: since they are much smaller than relevant gradients in n_e, B and T (except possibly in the vicinity of current sheets), these physical properties may be regarded as constant across any given gyroresonant layer.

The expression for the optical depth τ of a gyroresonance layer (the absorption coefficient integrated through the layer) as a function of the frequency f, the harmonic number s (which determines $f_B = f/s$ and hence B in the layer), and the angle θ between the magnetic field direction and the line of sight is (Zheleznyakov, 1970; Melrose, 1980; Robinson & Melrose, 1984):

$$\tau_{x,o}(s,f,\theta) \;=\; .0133\,\frac{n_e L_B(\theta)}{f}\,\frac{s^2}{s!}\left(\frac{s^2\,\sin^2\theta}{2\mu}\right)^{s-1} F_{x,o}(\theta) \tag{1}$$

where $L_B(\theta)$ is the scale length of the magnetic field $(B/\frac{\partial B}{\partial l})$ evaluated along the line of sight. For simplicity we have set the refractive index to be unity in (1). $F_{x,o}(\theta)$ is a function of angle which is of order unity for the x mode near $\theta = 90^\circ$, but decreases sharply at smaller θ, and is smaller in the o mode than in the x mode. At angles θ away from 90° it is often approximated by

$$F_{x,o}(\theta) \;\approx\; \left(1 - \sigma\cos\theta\right)^2 \tag{2}$$

with $\sigma = -1$ for the x mode and $\sigma = 1$ for the o mode. However, this approximation is really only appropriate

when the two natural electromagnetic modes are perfectly circularly polarized, and at the low harmonics (s = 1,2,3,4) relevant to the corona this is rarely a good assumption.

A summary of the properties of gyroresonance emission follows:

- For typical coronal conditions, the x mode is optically thick ($\tau \geq 1$) in the s = 2 and 3 layers over a broad range of angles θ. The o mode is optically thick over most of the s = 2 layer, and may be at least marginally optically thick over a small portion of the s = 3 layer if θ is large. Harmonics greater than s = 4 do not have any significant optical depth in the quiet solar corona.
- At each harmonic and angle the o mode opacity is always at least an order of magnitude smaller than the x mode opacity, despite the fact that (2) predicts that they should be nearly equal for a range of θ around 90°. The approximation (2) is adequate for the x mode at small θ, but is poor for the o mode at all θ, being easily a factor of 2 or more in error even at small angles.
- The opacity drops sharply towards small θ in both modes. By (1), the opacity is zero at θ = 0° for $s > 1$. The $\sin^{2s-2}\theta$-dependence of (1) causes the fall-off towards small θ to be much more rapid as s increases.
- For each increase of s by 1, the opacity in a given mode at a given angle drops by slightly more than 2 orders of magnitude. This is largely due to the μ^{-s} dependence of (1). The importance of this large change in opacity from one layer to the next is that a given harmonic layer is likely to be either optically thick over a wide range of angles θ, or else optically thin everywhere.

An important point to be emphasized is that gyroresonance observations are sensitive to the absolute magnetic field strength B, whereas conventional (Babcock or Leighton style) optical magnetographs measure only the line-of-sight component of the magnetic field, $B_l = B\cos\theta$, and thus are of limited value for regions near the solar limb. Further, in many cases magnetographs measure magnetic flux averaged over a resolution element (a pixel or a seeing cell) and are thus affected by the filling factor of the magnetic field within the resolution element; radio measaurements of B are not affected by this filling factor.

3. GYRORESONANCE EMISSION FROM ACTIVE REGIONS

Here we will use a dipole magnetic field (vertically-oriented and seen looking directly onto one pole, often used as a model for isolated sunspots) to illustrate the ways in which the properties of gyroresonance emission affect the appearance of solar active regions at microwave frequencies. Figure 3 shows the expected appearance of a perfectly dipolar field (of peak surface field strength 2500 G) at a frequency of 5 GHz. The upper panel shows the four lowest gyroresonant layers (s = 1, 2, 3, 4, corresponding to B = 1785, 892, 595 and 446 G, respectively), with the line-type indicating whether the layer is optically thick in a given mode. A solid line in the upper panel indicates that the layer is optically thick at both x and o modes; a dashed line indicates that only the x mode is optically thick; and a thin dotted line represents a region of the layer optically thin in both modes. The thin solid lines are magnetic field lines. In the bottom panel we plot the brightness temperature seen by an observer looking straight down on the dipole. In this panel the solid line represents the x mode brightness temperature, which the observer will see as one circular polarization (right circular polarization if the spot is of positive magnetic polarity), while the dashed line represents the o mode (seen by

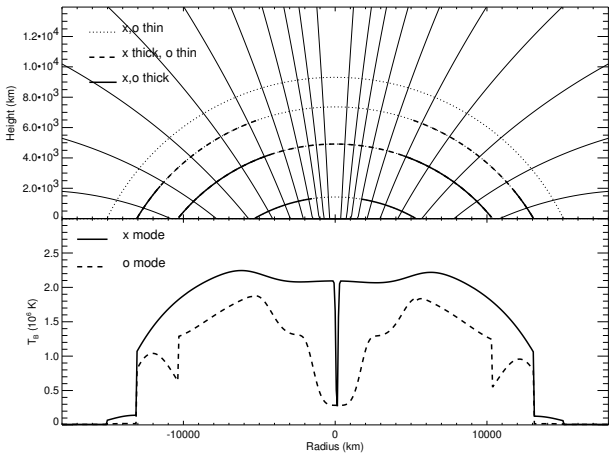

Figure 3. Plots of the gyroresonance layers of a dipole sunspot model (upper panel) and the predicted brightness temperatures resulting from an observation of such a spot (lower panel), viewed nearly vertically (actually 1° off vertical). In the upper panel the thin solid lines are magnetic lines of force and the dotted lines are the $s = 1, 2, 3, 4$ gyroresonance layers, with $s = 4$ the highest and $s = 1$ the lowest layer. Where the gyroresonance layers are optically thick (i.e., $\tau \geq 1$) in the o mode, they have been overplotted with a thick solid line. Except in the $s = 1$ layer where the x mode does not propagate, a layer which is optically-thick in the o mode is also thick in the x mode. If a gyroresonance layer is optically thick in the x mode but not in the o mode, it is overplotted with a thick dashed line. In the lower panel, the x-mode brightness temperature is shown by a solid line and the o mode brightness temperature by a dashed line. The frequency is 5.0 GHz, the dipole is buried at a depth of 1.2×10^9 cm, and the maximum field strength at the surface is 2500 G. In the model temperature increases with radial height from 1.0×10^6 K at the base of the corona (zero height in this case) to 3.0×10^6 K at about 15000 km.

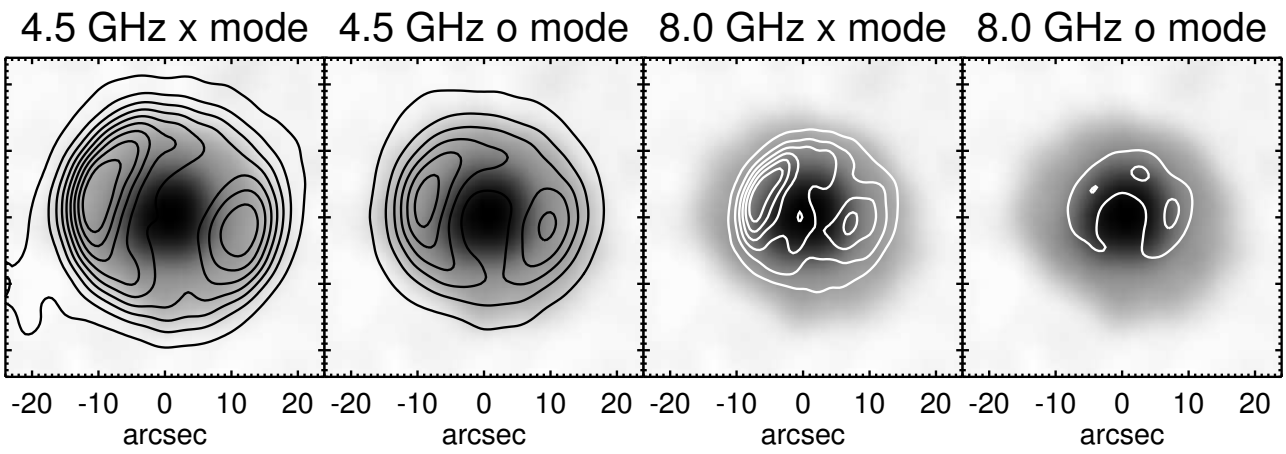

Figure 4. Radio contours (at two frequencies in each sense of circular polarization) plotted over a white light image of a sunspot for a particularly simple spot observed close to disk center with the Very Large Array on 1994 October 15. Contours are plotted at brightness temperatures of 1,3,5,7... $\times 10^5$ K. 4.5 GHz corresponds to a magnetic field strength of 540 G if emission is at s = 3, while 8.0 GHz corresponds to 950 G. The radio emission is low over the center of the spot where we are looking nearly parallel to the magnetic field direction in the corona and the opacity is low, whereas at the outer edge of the spot the opacity is high because θ *is larger and optically thick radio emission at coronal temperatures is observed.*

the observer as the opposite circular polarization).

A height of zero in the atmospheric model used for this calculation corresponds to the base of the corona. The density is 10^{10} cm^{-3} at the base and decreases exponentially with a scale height of 5000 km. The temperature is 6000 K below the corona and 1.0×10^6 K at the base, increasing to 3.0×10^6 K at a height of about 15000 km. The morphology of the radio emission can easily be understood by referring to the gyroresonance (GR) layers and the details of the temperature model, and recalling that along any given line of sight we only see down to the highest optically thick layer:

- Neither mode is optically thick in the $s = 4$ layer, but at the outer edges of this layer there is enough opacity in the *x* mode to produce a brightness temperature of order 10^5 K, which provides the outer boundary of the radio source.

- On the $s = 3$ layer, the *o* mode is only (marginally) optically thick at the low-lying outer edge of the layer where θ is largest, but the temperature is relatively low there because of the low altitude. The *x* mode is optically thick in the $s = 3$ layer to within $\sim$ 5000 km from the center of the umbra, and the peak brightness temperature in the *x* mode occurs close to the inner edge of this optically-thick region since the height of the layer, and therefore the temperature, is maximum there.

- At smaller radii where the $s = 3$ layer is optically thin, the main contribution to the *x* mode comes from the $s = 2$ layer which is lower and therefore at a lower temperature: this shows up as a drop in brightness temperature at small radii.

- In the very center of the $s = 2$ layer where the line-of-sight is along the field line, the *x* mode is optically thin and there is a narrow low-temperature feature. However, it is only a fraction of an arcsecond across and would be difficult to observe.

- In the *o* mode the central depression in brightness temperature due to the transparency of the $s = 2$ layer at small θ is much broader, and at the center of the spot even the $s = 1$ layer is optically thin in the *o* mode, but still has sufficient opacity to maintain the brightness temperature at 3.0×10^5 K.

- The sharp features in the *o* mode profile at radii of order 10^4 km are due to the gap between the radius at which the optically thick $s = 2$ layer drops beneath the corona and the radius at which θ increases sufficiently for the $s = 3$ layer to become (in this case only marginally) optically thick.

An example of the observed radio emission from a sunspot near disk center is shown in Figure 4 and it does in general terms reproduce the properties shown by the model sunspot. The outer boundary of the bright radio emission is much larger at 5 than at 8 GHz, because the field strength needed to make the corona optically thick is smaller at 4.5 GHz (540 G) than at 8.0 GHz (950 G). The emission drops off in the center of the spot where we are looking along the magnetic field and opacity drops; at the same time, the temperature in the corona over the center of the umbra is lower than it is over the penumbra. In the *o* mode images (at both frequencies) the hole in the center of the radio source is much more prominent than in the *x* mode due to the lower opacity of the *o* mode. Observations such as these confirm our understanding of the gyroresonance mechanism, and so we can use it to determine coronal magnetograms.

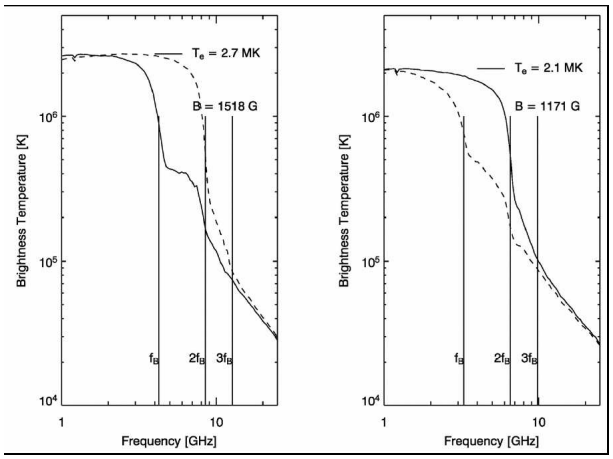

Figure 5. Radio spectra at two locations in the radio emission from an active region model of Mok et al. The solid and dashed lines correspond to the two senses of circular polarization. The two polarizations are optically thick in different harmonic layers. The edges (in frequency) where the optically thick layer drops below the transition region can be identified by the dramatic drop in brightness temperature: from the ratio of the edge frequencies in the two modes, the harmonic numbers of the corresponding gyroresonance layers can be identified and the magnetic field strength can be identified unambiguously.

Comparison of high–quality radio observations of gyroresonance emission from active regions with extrapolations of surface magnetic field observations have been shown to be a powerful approach to understanding coronal magnetic fields. Lee et al. (1997) showed that active regions with strong shear display coronal gyroresonance radio sources that cannot be explained by potential–field extrapolations of photospheric magnetograms, confirming that coronal currents influence the coronal magnetic field in ways that show up directly in the radio images. Lee et al. (1998) then showed that a nonlinear force–free extrapolation of a high–quality vector magnetogram could satisfactorily reproduce these sources, and further showed that the temperature in the corona could be linked to the presence of coronal currents. Lee et al. (1999) compared the temperature measured on the same magnetic field line at two different radio frequencies, corresponding to two different heights in the corona, and showed that the temperatures are well correlated for field lines determined from the nonlinear force–free extrapolation but not from any other approach. These studies show the value of comparisons of direct measurements of B from radio data with extrapolations of surface fields.

4. CORONAL MAGNETOGRAPHY

It is important to note that coronal magnetic fields are intrinsically a three–dimensional problem, unlike photospheric magnetic fields, and thus they require a different mindset. Optically thin diagnostics have line-of-sight problems to deal with; here radio has an advantage because it is optically thick, so that we get different layers of the corona at different radio frequencies. Extrapolations of surface fields will continue to be crucial because the radio observations dont measure the height of the gyroresonance layers (just as optically–thin diagnostics don't measure the position of a source along the line of sight), so the radio data do not provide absolute height information (although they do provide some relative height information). Extrapolations of surface fields can use radio measurements to help resolve ambiguities and issues with non-force-free photospheric field data. But for radio measurements to be useful we need a telescope that makes high-quality, high-resolution maps of the Sun at many frequencies simultaneously, to measure a wide range of magnetic field strengths.

The Frequency Agile Solar Radiotelescope (FASR) project is designed to be such a telescope (Bastian, 2003; Gary, 2003; Bastian, 2004). It will be a multi–element ($\sim$ 100 antennas), multi–frequency (0.02–24 GHz) array designed specifically to observe the Sun. FASR will produce high spatial resolution images ($1''$ at 20 GHz) of the full solar disk at many closely–spaced frequencies with high time resolution ($\sim$ 1 second). FASR will produce a continuous 3D picture of the solar atmosphere from the chromosphere up into the mid corona.

Gary et al. (2005) have now demonstrated the method for measuring the magnetic field strength at the base of the corona from realistic data of the type that FASR will provide. The technique rests on two facts: (i) Along any given line of sight the corona will be optically thick and show MK brightness temperatures up to a frequency determined by the maximum field strength in the corona, which usually will occur at the base of the corona. At higher frequencies the optically thick layers lie below the transition region and produce lower brightness temperatures, so sharp edges will be seen in frequency spectra of the brightness temperature. (ii) The problem then is determining which harmonic number an edge corresponds to: s = 2, 3 or 4. To solve this problem we use the fact that except when **B** is orthogonal to the line of sight (in which case likely s=3), the two circular polarizations will be optically thick at different harmonics and thus have edges at different frequencies. Because we only have a limited range of harmonics to consider, the ratio of the edge frequencies in the two polarizations will be a rational number that unambiguously determines the harmonics for both polarizations.

Gary et al. (2005) have used a model active region developed by Mok et al. (2005) to test this method. The results are shown in Figs. 5 & 6. The model consists of a coronal magnetic field extrapolated from a photospheric vector magnetogram with temperature and density specified self–consistently throughout the corona using a heating model with a volumetric heating rate proportional to the local value of B. This model was folded through a radiative transfer code that calculated the gyroresonance and bremsstrahlung emission at a large number of closely–

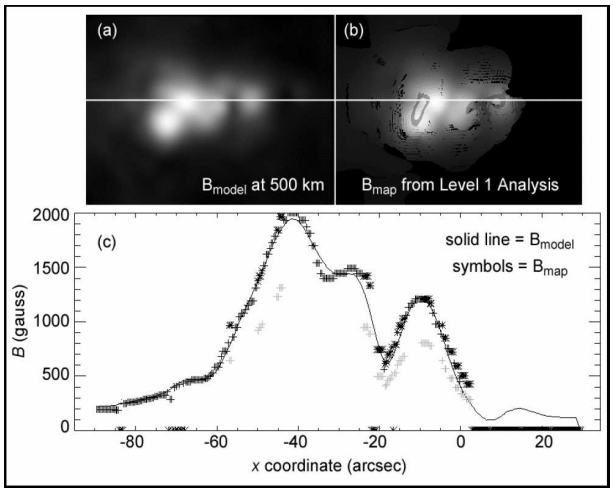

Figure 6. (Lower panel) Comparison of the determination of the magnetic field strength at the base of the corona along a cut across the model active region with the actual field strengths in the input model. This is a realistic experiment using the technique described above, and shows that the high frequency resolution imaging data provided by FASR will produce coronal magnetograms routinely. The two upper panels are greyscale representations of the magnetic field input model (left) and radio–derived measurement (right): the location of the cut is shown by the white line. Improvements in the analysis technique such as continuity arguments should be able to clean up areas where the method did not work as well due to, e.g., the two edges being at the same harmonic.

spaced frequencies, and the resulting radio models were "observed" by convolving them with real telescope response functions and then carrying out the deconvolution exactly as FASR will do. Fig. 5 shows radio brightness temperature specta at two locations, with edges clearly visible at different frequencies in the two polarizations. Using these edges we can identify B at the base of the corona in every pixel in the image where gyroresonance emission makes the corona optically thick. In Figure 6 we compare the radio–measured magnetic field strengths with the actual input model values for a cut across the region, showing how well the technique works.

In summary, gyroresonance measurements yield the following results for coronal magnetography:

- Radio observations can measure coronal magnetic field strengths above 300 G anywhere in the solar corona
- The technique measures temperatures on surfaces of constant field strength, so it directly sees regions of strong heating in the corona.
- Because emission is optically thick in regions of strong fields, we get 3D information on fields.
- The technique is relatively insensitive to density, and therefore complements other techniques which are dominated by density contrast
- Presently no absolute height information can be obtained directly from the radio data: here information from other wavelengths may be helpful.
- These measurements will play an important role in testing techniques for extrapolating surface fields into corona.

5. OTHER METHODS

As noted earlier, since the presence of a magnetic field alters the properties of the coronal plasma it leaves its imprint on all the emission mechanisms and in principle they all contain information on the coronal field that can be exploited. We mention some of the possibilities here, but this is by no means an exhaustive list: more comprehensive information may be found in the volume by Gary & Keller (2004).

5.1. Gyrosynchrotron emission from flares

Mildly relativistic electrons located in magnetic fields are very efficient producers of radio emission due to the gyrosynchrotron mechanism. This fact, combined with our ability to make high spatial resolution images at radio wavelengths, provides a powerful technique to study energy release and electron acceleration processes in solar flares *from the ground*, in contrast to hard X-ray/γ-ray studies which require space platforms. In addition to fundamental morphological information on the location of the nonthermal electrons and their behaviour, multifrequency radio observations can be used to study quantitatively the physical conditions inside the flare source, thanks to the fact the we understand the emission mechanism well (Dulk, 1985; Bastian et al., 1998). Flares may show distinct loop shapes in which nonthermal electrons are radiating as they mirror back and forth between strong magnetic fields at the loop footpoints at the surface (e.g., Figure 7: however many flares do not show obvious loops in radio images). At any given location in the flare source, the location of the peak in the radio spectrum depends almost linearly on the magnetic field strength there and only weakly on other parameters; this property is illustrated in Figure 8. The spectral index on the high-frequency side of the spectral peak reveals the energy spectral index of the radiating electrons; the degree of polarization of the radio emission indicates the local direction of the magnetic field; and the number density of nonthermal electrons can also be determined from measurements at several frequencies. Thus spatially resolved imaging spectroscopy can reveal the complete set of physical parameters describing flare sources, but the power of this method can only be exploited with a telescope that can provide high-resolution imaging across a broad frequency range quasi-simultaneously. This technique is another major science objective for FASR.

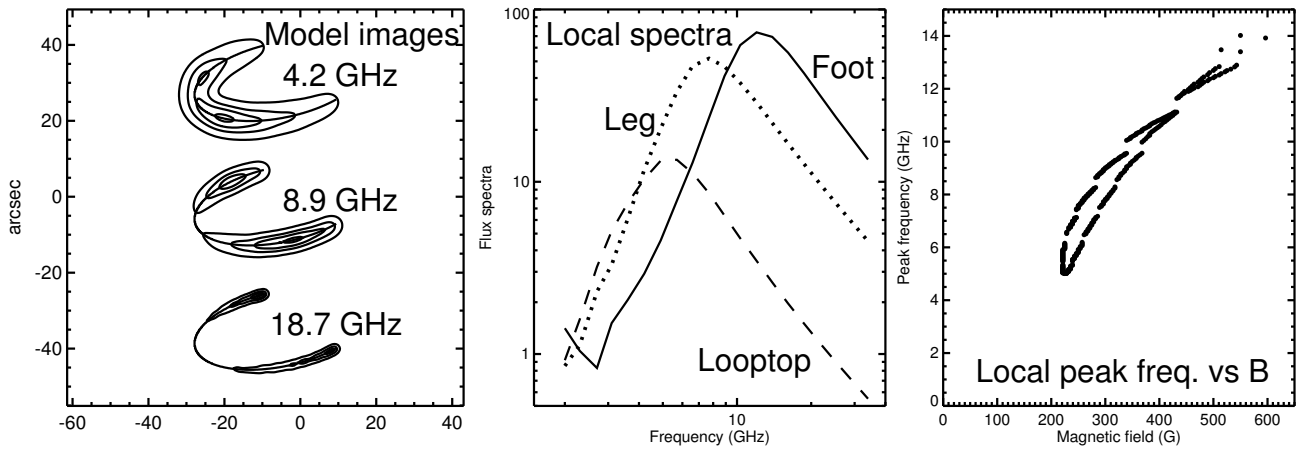

Figure 8. Gyrosynchrotron emission from a model coronal magnetic loop. The panel at left shows how the appearance of the loop changes from low optically thick frequencies (4.2 GHz), where the loop top dominates, to high optically thin frequencies (18.7 GHz), where the footpoints dominate because of the stronger magnetic fields there. The thin solid line indicates the spine of the loop in each case. In the middle panel are plotted local radio spectra at three different locations within the loop: at a footpoint (solid line), at the top of the loop (dashed line), and at a location half-way up the leg of the loop (dotted line). In the right panel we plot the frequency of the peak of the radio spectrum versus the local magnetic field, showing that there is a nearly linear dependence of the spectral peak on the local magnetic field and thus spatially-resolved spectroscopy can be used to measure the variation of magnetic field along the loop.

5.2. Polarization of bremsstrahlung emission

As noted earlier, the radio emission from the quiet Sun is dominated by bremsstrahlung emission. The contrast visible in images such as Fig. 1 is due to optically thin density contrast in the corona, exactly as in soft X–ray images. Figure 9 shows that the circular polarization of this optically thin bremsstrahlung can be detected with present instruments, so it does offer a possible diagnostic. The theory of optically thin bremsstrahlung polarization is well understood (e.g., Gelfreikh, 2004): the degree of polarization P is effectively proportional to B_l, $P = 2\,(f_B/f)\cos\theta$.

In the case of optically thick bremsstrahlung, the polarization is due to the fact that the opacity of the two natural modes is different so that they become optically thick in layers with slightly different temperatures. The difference in temperature between the layers shows up as polarized flux. The fact that the polarization in this case is due to a temperature gradient would suggest that it cannot be used to determine the magnetic field properties, but Grebinskij et al. (2000) have shown that the technique still works. The basic idea is that the radio spectrum itself measures the temperature gradient, which is the quantity needed to determine the longitudinal magnetic field B_l. Provided one has sufficiently dense (in frequency) measurements of the brightness temperature spectrum, the local slope of the free–free emission brightness temperature spectrum, $m = dlog(T_e)/dlog(f)$, can be determined and the expression for the measured degree of polarization becomes $P = m\,(f_B/f)\cos\theta = m\,(2.8\times10^6/f)\,B_l$. Thus, $B_l = Pf/(2.8\times10^6 m)$ where all the quantities on the right hand side are measured. Dale Gary has carried out tests of the technique and with ideal model data it reproduces the longitudinal magnetic field well. When more realistic data are used, including noise, discrete frequency sampling and the fact that the spatial resolution is proportional to the wavelength, then the determination of m can be noisy, so that very high quality data may be needed to exploit this approach extensively.

5.3. Plasma emission

Plasma emission is also polarized because the conversion of the electrostatic Langmuir waves depends on the properties of the natural modes of the plasma, which in turn depend on the magnetic field even though it is generally weak in typical sources of plasma emission. Emission at the fundamental of the plasma frequency should be 100% polarized in the sense of the o mode in a magnetized plasma because the x mode is cut off at a frequency above f_p. The polarization of second harmonic plasma emission formed by coalescence of two oppositely–propagating Langmuir waves is also understood (Zlotnik, 1981).

Figure 10 illustrates another example of using plasma emission to measure coronal fields (Aurass et al., 2005). "Fiber bursts" appear in some complex solar radio bursts as narrow fine structure that drifts in frequency with time within broadband emission in the decimeter wavelength range. A model for these bursts invokes whistler waves ascending post–flare coronal loops and acting as magnetic traps for nonthermal flare electrons. The whistler frequency can be derived from the pattern of emission ridges and absorption channels in the dynamic spectrum: adjacent emission ridges are assumed to be separated by the whistler frequency. Since the emission mechanism is believed to be plasma emission, the ambient elec-

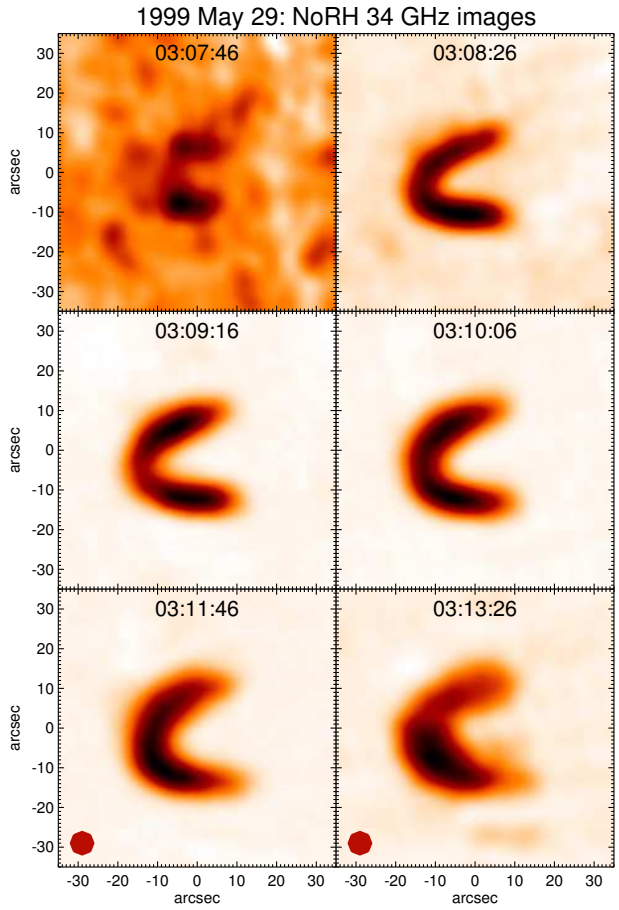

Figure 7. Images of a flare on 1999 May 29 observed by the Nobeyama Radio Heliograph at 34 GHz. This was a simple loop flare in which the loop shape remained steady but some loop parameters, notably length and footpoint separation, evolved with time, and shifts in the location of brightness maxima were seen (White et al., 2002).

tron density is simply determined from f_p. Knowing the whistler frequency and n_e then allows B to be determined. Aurass et al. (2005) compared the resulting fields at locations known from the imaging data with magnetic field strengths determined from an extrapolation of surface fields and found good consistency between the two methods.

6. SUMMARY

Coronal magnetic field measurements will become greatly improved over the next decade. Optical and IR measurements will be carried out at moderate spatial resolution off the solar limb. Because they need to be off the limb, they will generally not see strong magnetic fields, and the measurements are difficult to compare with surface fields because of projection effects. Optically thin diagnostics will suffer from line of sight confusion issues and will be dominated by the densest features along any line of sight, but offer the possibility of full Stokes measurements.

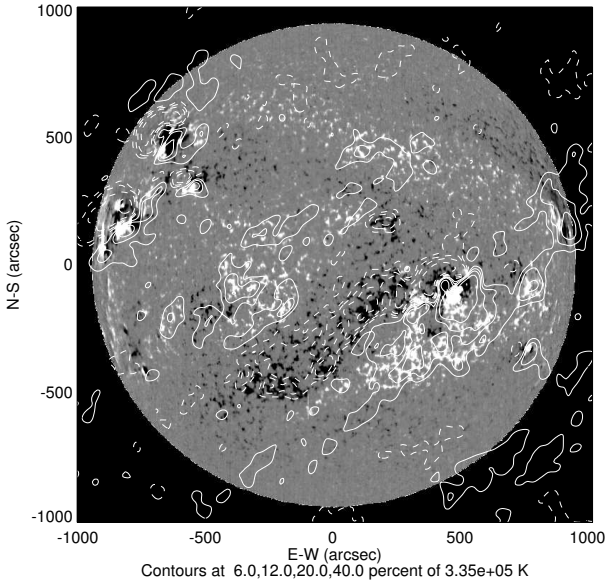

Figure 9. Contours of circularly polarized radio emission at 1.4 GHz (map from the Very Large Array, 1991 May 7; positive contours show positive Stokes V or right circular polarization, dashed contours show left circular polarization) overlaid on a Kitt Peak magnetogram. The display range on the magnetogram is -100 to 100 G. Note that in regions of plage the extended polarized radio emission matches the underlying magnetic field in direction: dashed contours over negative B, solid contours over positive B.

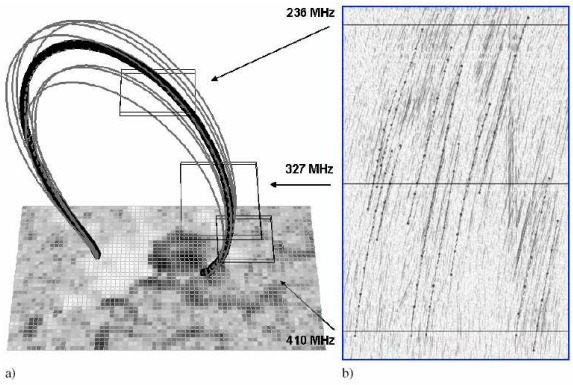

Figure 10. "Fiber" bursts used to measure the coronal magnetic field. The panel at right shows a dynamic spectrum (frequency on the vertical axis, 60 s of time on the horizontal axis) with fitted fiber–burst traces over–plotted. At left is a photospheric magnetogram with field lines, computed via a potential extrapolation of surface fields, that pass through the source regions at different frequencies (boxes, with arrows from the corresponding frequencies in the dynamic spectrum) identified from images made with the Nancay Radioheliograph.

Radio measurements by the gyroresonance technique are sensitive to the absolute magnetic field strength and line-

of-sight orientation for field strengths above 100 G (lower field strengths correspond to low frequencies where other sources of opacity tend to take over). Therefore the radio gyroresonance method really only works for active regions, but has the great advantage that it works on the disk, and thus is available for comparison with surface fields. However it does not see weak fields, so misses magnetic flux associated with weak coronal fields that may still play an important role in the corona. Bremsstrahlung polarization may offer better information on weak fields in the corona but it is not as precise as gyroresonance measurements. Three–dimensional information is present in the radio data, but absolute heights are not measured. Spatial resolution in the radio domain scales inversely with B. Both the radio and optical/IR measurement methods will be compared extensively with extrapolations from surface magnetograms, preferably from chromospheric vector magnetograms when available.

ACKNOWLEDGEMENTS

Solar research at the University of Maryland is supported by NSF grant ATM 02-33907 and NASA grants NAG 5-10175, NAG 5-12860, NAG 5-12732, NAG 5-11872, and NNG05GI91G.

REFERENCES

Aurass, H., Rausche, G., Mann, G., & Hofmann, A. 2005, Astron. Astrophys., 435, 1137

Bastian, T. S. 2003, in Innovative Telescopes and Instrumentation for Solar Astrophysics (Proceedings of the SPIE, Volume 4853), ed. S. L. Keil & S. V. Avakyan, 98–110

Bastian, T. S. 2004, in Solar and Space Weather Radiophysics, ed. D. E. Gary & C. U. Keller (Dordrecht: Kluwer Academic Publishers), 47–69

Bastian, T. S., Benz, A. O., & Gary, D. E. 1998, Ann. Rev. Astron. Astrophys., 36, 131

Dulk, G. A. 1985, Ann. Rev. Astron. Astrophys., 23, 169

Gary, D. E. 2003, Journal of Korean Astronomical Society, 36, 135

Gary, D. E. & Keller, C. U. 2004, Solar and Space Weather Radiophysics - Current Status and Future Developments (A&SSL Vol. 314) (Dordrecht: Kluwer Academic Publishers)

Gary, D. E., Lee, J., Giordano, G., & Mok, Y. 2005, Astrophys. J., in preparation

Gelfreikh, G. B. 2004, in Solar and Space Weather Radiophysics, ed. D. E. Gary & C. U. Keller (Dordrecht: Kluwer Academic Publishers), 115–133

Grebinskij, A., Bogod, V., Gelfreikh, G., Urpo, S., Pohjolainen, S., & Shibasaki, K. 2000, Astron. Astrophys. Supp. Ser., 144, 169

Lee, J., McClymont, A. N., Mikić, Z., White, S. M., & Kundu, M. R. 1998, Astrophys. J., 501, 853

Lee, J., White, S. M., Gopalswamy, N., & Kundu, M. R. 1997, Solar Phys., 174, 175

Lee, J., White, S. M., Kundu, M. R., Mikić, Z., & McClymont, A. N. 1999, Astrophys. J., 510, 413

Melrose, D. B. 1980, Plasma Astrophysics (New York: Gordon and Breach)

Mok, Y., Mikić, Z., Lionello, R., & Linker, J. A. 2005, Astrophys. J., 621, 1098

Robinson, P. A. & Melrose, D. B. 1984, Aust. J. Phys., 37, 675

White, S. M., Kundu, M. R., Garaimov, V. I., Yokoyama, T., & Sato, J. 2002, Astrophys. J., 576, 505

Zheleznyakov, V. V. 1970, Radio Emission of the Sun and the Planets (Oxford: Pergamon Press Ltd.)

Zlotnik, E. I. 1981, Astron. Astrophys., 101, 250